Optics Letters

Few-cycle pulse generation by double-stage hybrid multi-pass multi-plate nonlinear pulse compression

Anne-Lise Viotti,[1,2] Chen Li,[1] Gunnar Arisholm,[3] Lutz Winkelmann,[1] Ingmar Hartl,[1] Christoph M. Heyl,[1,4,5] and Marcus Seidel[1,*]

[1]Deutsches Elektronen-Synchrotron DESY, Notkestr. 85, 22607 Hamburg, Germany
[2]Department of Physics, Lund University, P.O. Box 118, SE-221 00 Lund, Sweden
[3]FFI (Norwegian Defence Research Establishment), P.O. Box 25, NO-2027 Kjeller, Norway
[4]Helmholtz-Institute Jena, Fröbelstieg 3,07743 Jena, Germany
[5]GSI Helmholtzzentrum für Schwerionenforschnung GmbH, Planckstrasse 1, 64291 Darmstadt, Germany
*Corresponding author: marcus.seidel@desy.de

Received 21 October 2022; revised 16 December 2022; accepted 19 December 2022; posted 19 December 2022; published 10 February 2023

Few-cycle pulses present an essential tool to track ultrafast dynamics in matter and drive strong field effects. To address photon-hungry applications, high average power lasers are used which, however, cannot directly provide sub-100-fs pulse durations. Post-compression of laser pulses by spectral broadening and dispersion compensation is the most efficient method to overcome this limitation. We present a notably compact setup which turns a 0.1-GW peak power, picosecond burst-mode laser into a 2.9-GW peak power, 8.2-fs source. The 120-fold pulse duration shortening is accomplished in a two-stage hybrid multi-pass, multi-plate compression setup. To our knowledge, neither shorter pulses nor higher peak powers have been reported to-date from bulk multi-pass cells alone, manifesting the power of the hybrid approach. It puts, for instance, compact, cost-efficient, and high repetition rate attosecond sources within reach.

https://doi.org/10.1364/OL.478790

Few-cycle pulses have pushed the frontiers of nonlinear optics far beyond the perturbative regime. The (temporary) detachment of electrons from the nuclei by strong fields leads to the creation of large dipole moments [1]. The atomic polarization is switched by few-cycle pulses on sub-femtosecond time scales without prior distortions of the interacting matter [1]. Many unique applications emerged, most prominent, the generation of coherent extreme ultraviolet or X-ray radiation and its temporal confinement to attosecond durations [2]. This, in turn, enabled tracking of ionization dynamics and performing electron microscopy with highest temporal and spatial resolution [3,4]. Beyond that, few-cycle pulses prospectively enable PHz bandwidth signal processing in solids [5,6]. Initial few-cycle sources relied on broadband laser gain media that are difficult to scale in average power [1]. However, high pulse repetition rates are important to achieve good signal-to-noise ratios despite the low efficiencies of extremely nonlinear processes or limitations caused by Coulomb interactions after ionization [4]. The advancement of ultrafast lasers in the past years to substantially higher average powers [7] has allowed the repetition rate shortcoming of few-cycle sources to be overcome, but has also imposed the challenge to reduce the inherent pulse durations of power-scalable lasers from hundreds or thousands of femtoseconds to the sub-10-fs regime. One approach to accomplish this is optical parametric amplification [8]. It provides wavelength tunability and excellent pulse contrast but is a relatively inefficient, complex method. Alternatively, spectral broadening and pulse post-compression present a direct, cost-efficient path to the few-cycle regime [9]. In particular, the multi-pass cell (MPC) spectral broadening technique has combined large pulse compression factors, i.e., the input to output pulse duration ratios, and high power efficiencies in an outstanding manner [10–12]. Recently, several few-cycle pulse generation schemes by means of MPCs have been reported [13–17]. All experiments were based on gas-filled MPCs which require at least approximately 100 MW of peak power and a sealed chamber that needs to be filled with nonlinear gas. In contrast, bulk material based few-cycle or even single-cycle pulse generation was demonstrated by the multiple plate continuum approach [18–21]. We have recently shown that combining the multiple plate and the bulk MPC techniques can clearly overcome the compression factors that are achievable by the methods alone in a single stage [22,23]. Here, we apply the hybrid approach to demonstrate more than hundred times pulse duration reduction, that is, from the picosecond regime to 8.2-fs FWHM duration. Moreover, we report the first bulk-based MPC that delivers sub-10-fs pulses with multi-GW peak powers.

The setup was based on an Yb:YAG laser and two spectral broadening stages [Fig. 1(a)], which enable to combine high efficiencies and large compression factors [11]. The laser and the first MPC stage (MPC 1) were similar to the setup reported in Ref. [22]. The main amplifier emitted laser bursts every 100 ms with a variable number of pulses and a 1-MHz pulse repetition rate. We adjusted the number of pulses to the dynamic range of our measurement devices and typically worked with 150–200 pulses per burst. The available pulse energy was 128.5 μJ and the compressed pulse duration 1 ps. MPC 1 consisted of two

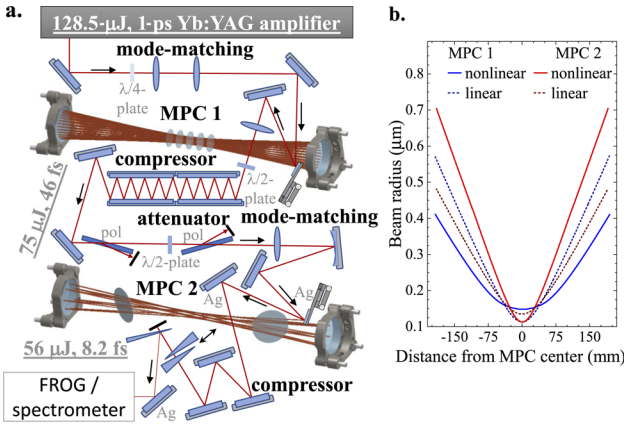

Fig. 1. (a) Two-stage pulse compression setup. Both MPC mirror pairs are separated by approximately 38 cm. The compressor and MPC 2 mirrors were chirped. The silver mirrors are denoted by Ag. All other mirrors are quarter-wave stacks. Thin-film polarizers (pol) are used. (b) ABCD matrix beam size predictions in MPCs 1 and 2 for mode-matching in the presence (nonlinear) and absence (linear) of the Kerr effect. In the presence of self-focusing, the beam radius on the mirrors in MPC 1 was reduced by approximately 30% and increased in MPC 2 by approximately 15% in relation to Kerr lens-free mode-matching.

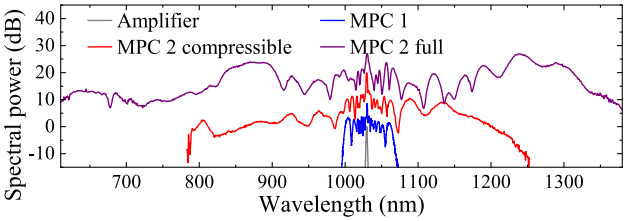

Fig. 2. Yb:YAG amplifier spectrum measured with a compact grating spectrometer compared to the broadened spectra after MPCs 1 and 2 which were measured with an optical spectrum analyzer (OSA). Red and violet lines represent two different MPC 2 settings. Narrower spectrum resulted in the shortest pulses, the broader spectrum covered the full mirror bandwidth. Spectra are offset for the sake of clarity.

quarter-wave stack dielectric mirrors with 200-mm radius of curvature (ROC) and five 1-mm-thin anti-reflection coated fused silica (FS) substrates. After 29 round trips in the MPC and 68 reflections from chirped mirrors with −200-fs^2 group delay dispersion (GDD), the pulses were compressed to 46 fs [Figs. 3(a) and 3(d)], close to the 43-fs Fourier transform limit (FTL) of the MPC 1 output spectrum (Fig. 2, blue line). We used input pulses longer than 1 ps to get the best compression after MPC 1 at the full input power. This resulted in a pulse energy of 75 µJ available for few-cycle pulse compression. The drawback of this configuration was an increase of the M^2-parameter from 1.1 to 1.5 after MPC 1 (Table 1), which we related previously to parasitic four-wave mixing [22]. For 1-ps pulse duration and 96.5-µJ energy at the MPC 1 input, we compressed the pulses to 45 fs while maintaining clearly better M^2-values of approximately 1.3 (Table 1). In this configuration, 61.5-µJ pulses could be sent into MPC 2.

To accomplish the large compression factors in MPC 1, we used nonlinear mode-matching. That means, we adjusted the

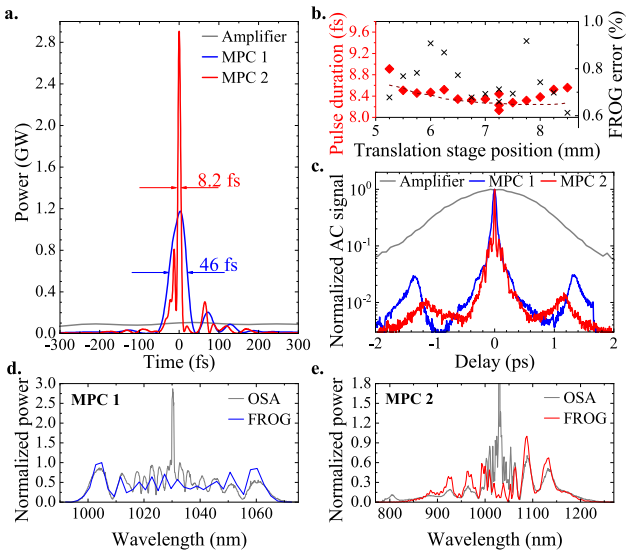

Fig. 3. (a) Retrieved pulses by FROG from the amplifier and after both compression stages. The 1-ps-long amplifier pulses are only partially shown on the time axis. (b) Retrieved pulse durations (red diamonds) and FROG errors (black crosses) for different amounts of glass in the beam path. A glass wedge with 12° apex angle on a translation stage was moved in 250-µm steps, corresponding to approximately 1-fs^2 GDD difference. The dashed line is computed from the electric field of the best retrieved pulse (translation stage position 7.25 mm) and the theoretical dispersion of the inserted glass. (c) Autocorrelation (AC) signal extracted directly from the FROG scans. For MPC 2, a step width of 50 fs was set for the 10-ps delay range. (d),(e) Comparisons between the retrieved spectra after MPC 1/MPC 2 and the measured OSA spectra. To limit the FROG grid size to 1024^2, a delay range of 700 fs was scanned which explains why the spectral power of the retrieved near-center wavelengths is lower than in the OSA measurement.

Table 1. Results of the M^2-Measurements

	Amplifier	MPC 1[a]	MPC 1[b]	MPC 2[c]
M_x^2/M_y^2	1.16/1.13	1.43/1.56	1.28/1.32	1.45/1.58

[a] 128.5 µJ at MPC 1
[b] 96.5 µJ at MPC 1
[c] detection up to 1.1 µm.

distances and refractive powers of the mode-matching lenses under consideration of self-focusing in the nonlinear media [22]. The same was done for MPC 2. However, the relative beam size changes with respect to the linear mode-matching setting, which does not account for Kerr lensing, were opposite in both stages [Fig. 1(b)]. In MPC 1, the five FS plates near the cavity center formed a weak waveguide. Therefore, the beam size in the center was larger compared to the linear case. Details are provided in Ref. [22]. In contrast, MPC 2 hosted only two FS plates which were located closer to the MPC mirrors than to the cell center. Consequently, the Kerr effect virtually enhanced the refractive power of the MPC mirrors like in gas-filled MPCs [24]. We had to separate the 1-mm thin FS plates in MPC 2 by approximately 22 cm to preserve the compressibility of the pulses. This resulted in a B-integral of approximately 0.6π per round trip. Whereas large spectral broadening factors like in MPC 1 cannot be reached in MPC 2 due to the limited mirror bandwidth, the freedom of dispersion control by the MPC

mirrors makes the hybrid multi-pass, multi-plate approach very attractive for few-cycle pulse generation. The spectrum measured after 7 round trips of the 75-μJ, 46-fs pulses is plotted in Fig. 2 (red line). The corresponding 7.4-fs FTL was enabled by octave-spanning chirped mirrors (CMs, Laseroptik) with 200-mm ROC, which strongly reduced the net dispersion per pass in MPC 2. To suppress the GDD oscillations inherent to single broadband CMs, an MPC mirror pair with complementary dispersion design was used. The CMs were designed to compensate 3 mm of FS dispersion per bounce.

We characterized the compressed pulses by second harmonic frequency-resolved optical gating (FROG) with a 10-μm-thin BBO crystal. The dispersion-free FROG setup is described in Ref. [25]. The shortest pulse duration we retrieved was 8.2-fs FWHM [Fig. 3(a)] corresponding to more than 120 times overall reduction of the pulse duration taking the feasible 1-ps pulses from the amplifier as reference. A pair of glass wedges [Fig. 1(a)] was used to find the best compression point. We compared the retrieved pulse durations from multiple FROG traces at different wedge positions [Fig. 3(b)] and obtained very good consistency of the results, such that we infer a ±0.2-fs uncertainty of the 8.2-fs duration. To our knowledge, only bulk-MPCs with at least twice as long pulses were reported before [26,27]. We determined a pulse energy of 56 μJ after MPC 2. The corresponding 75% transmission of the stage included three bounces off silver mirrors. To minimize the reflection losses of the Kerr media, we placed the FS plates at Brewster's angle into MPC 2. Assuming 97.2% and 99.6% reflectivity of the silver and chirped mirrors, respectively, we deduce an average Fresnel loss of 0.5% per FS–air interface. This shows that polarization rotation due to out-of-plane propagation in the MPC is a minor concern. We attribute this to the tenfold ratio between MPC length and Herriott-pattern diameter. The CM reflectivities were calculated from the broadened spectrum and the mirror design. However, the experimental reflectivity per pass deduced from the transmission of the Kerr medium-free MPC 2 was on average 0.2% lower. Nevertheless, the >99% reflectivity of the CMs is an advantage over (enhanced) silver mirrors, which have so-far been used in all MPCs for sub-10-fs pulse generation [14–17]. We note that the CM design exhibits a 0.6% lower reflectivity at 1030 nm than at the wings of the spectrum after MPC 2. This helps to remove several percent of the residual narrowband radiation emitted by the Yb:YAG amplifier. In-fact, the autocorrelation traces of Fig. 3(c) show that a side pulse with 1–2-ps delay from the main peak is suppressed by 5 dB in comparison to pulses after MPC 1, which is also due to the peak power enhancement of the main pulse. From the pulse energy, the FROG retrieval, which covered a 700-fs delay range, and the autocorrelation measurement over a 10-ps range, we derive a peak power of approximately 2.9 GW which surpasses the present bulk-MPC record of 2.5 GW [28]. An enhancement to 3.5 GW is expected from third-order dispersion compensation which would also suppress the strongest side pulse to approximately 10% of the peak. The other pedestals stem from the pulse shapes of the amplifier and the first compression stage. Owing to the small net GDD per pass, we could readily broaden the pulse spectra to fully cover the CM reflectance band from approximately 0.6 μm to 1.4 μm. An experiment with 1-ps pulses from the laser, 45-fs, 61.5-μJ pulses from MPC 1, and only 12-cm distance between the Kerr media in MPC 2 yielded an octave-spanning spectrum with a single-cycle FTL (violet line in Fig. 2). The spectrum does not exhibit the blue shoulder caused by self-steepening in multiple

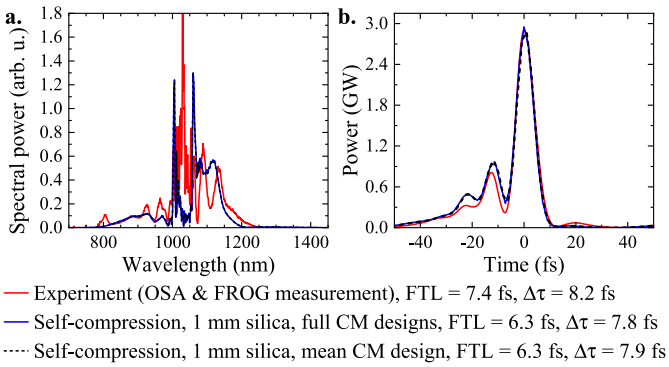

Fig. 4. (a) Experimental (red line) and simulated (blue/black lines) output spectra of MPC 2. The black dashed line included only averaged properties of the complementary CM pair. (b) Corresponding pulses. The pulses plotted with black and blue lines result from self-compression at the end of the seventh MPC round trip. Here, Δτ denotes pulse duration.

plate continua [18–21]. It is dominated by self-phase modulation, which was enabled by dispersion control through the CMs. The experiment was done with 12 round trips in MPC 2, which were less decisive for the broadening factor than the plate distance due to additional losses. However, higher intensities in the Kerr media yield spatiotemporal couplings. Consequently, a FROG measurement showed that it is not possible to compress the pulses close to the spectrum's FTL by the CMs we used. Tailored CMs could compensate for the characteristic bulk-broadening phase [29]. Alternatively, the use of thinner Kerr media, like in the multiple plate continuum method, promises to push achievable durations in MPC 2 toward the single-cycle regime [21].

Figure 4 compares the experimental results (red lines) with SISYFOS simulations [22,30] of MPC 2. The shortest pulses attainable for two 1-mm-thin FS plates were computed in the course of the seventh round trip through MPC 2 omitting the need for post-compression (blue and black lines in Fig. 4). The net anomalous dispersion was approximately -10 fs^2 per pass in the simulations. Three additional bounces from mirrors, coated like the MPC 2 CMs, for best compression indicate that the experimental net GDD per pass was closer to 0 fs^2. We attribute the small difference to the imprecise knowledge of the CM dispersion, which we did not measure. Nevertheless, the overall agreement between experimental and simulated spectra and pulse shapes is very good. We investigated if the GDD oscillations exhibited by a single CM are detrimental for pulse compression. The blue lines in Fig. 4 show the simulation results under consideration of both complementary mirror designs, whereas the black dashed lines show the results for considering only the averaged reflectivity and GDD of the CM pair. Only minor differences in spectrum and compressed pulse shapes are visible, and thus we conclude that the GDD oscillations of the CMs only marginally influenced the compression results. For the most part, the simulation methods are described in Ref. [22]. We additionally included the Raman response of FS and blueshifted the CM design by 2 THz owing to slightly lower deposition rates close to the curved mirror edges. The FROG retrieval from MPC 1 and a fundamental Gaussian were used as pulse and beam shapes, respectively. The simulated pulse energy was set to 33.4 μJ to match the experimental intensities in the Kerr media. These were lowered

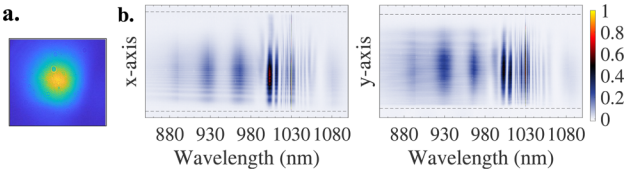

Fig. 5. (a) Profile and (b) spectral homogeneity of the beam behind MPC 2. The homogeneity was calculated like in Ref. [22] over the full width 0.5% maximum of the wavelength integrated power (dashed lines). It was 96.5% along the x axis and 97.5% along the y axis. The spectra had to be recorded over several grating positions of the spectrograph and stitched together in post-processing. The y-axis plot was rotated by 0.43° in post-processing of the data. The used Si-based cameras could not respond to wavelengths >1.1 μm.

by the ≈1.5 M^2-factor and Brewster's orientation which also increased the path through the FS plates by 21%. In our simulations, the intensities stay below 0.72 TW/cm^2 in the Kerr media of MPC 2. This is less than 10% of the typical intensities in few-cycle pulse generation with multiple thin plates only [18–21]. Consequently, the multi-photon ionization probability is strongly suppressed. Because of this and with reference to the discussions in [22], we expect power scalability of the hybrid multi-pass multi-plate approach akin to gas-filled MPCs [14,17], albeit the used burst laser cannot experimentally prove it.

The beam profile behind MPC 2 [Fig. 5(a)] does not show the ring structure which is characteristic for multiple-plate continua [18–21] and exhibits excellent spectral homogeneity despite Brewster's angle orientation of the Kerr media. By means of a 4f-imaging spectrograph [22,23], we determined that the horizontal (x) and vertical (y) beam axes exhibited >96% spectral homogeneity [Fig. 5(b)]. This is a typical MPC compression property. The measured M^2 values were nearly identical to the ones after MPC 1 (Table 1). In conclusion, we have turned a ps laser into a few-cycle light source by a sub-m^2 footprint two-stage hybrid multi-plate MPC setup that yielded a record-high more than 120-fold pulse duration shortening. The demonstrated multi-GW peak power is well suited for high harmonic generation and probing other strong field phenomena. With better phase control over the attainable octave-spanning spectra and the carrier-envelope offset, a compact MHz rate attosecond source is in reach.

Funding. Helmholtz Association; Vetenskapsrådet (2019-06275).

Acknowledgments. We thank Cord Arnold (Lund University) and Tobias Groß (LASEROPTIK) for fruitful discussions and DESY (Hamburg, Germany), a member of the Helmholtz Association HGF, for the provision of experimental facilities.

Disclosures. The authors declare no conflicts of interest.

Data availability. Data underlying the results presented in this paper are not publicly available at this time but may be obtained from the authors upon reasonable request.

REFERENCES

1. T. Brabec and F. Krausz, Rev. Mod. Phys. **72**, 545 (2000).
2. I. Orfanos, I. Makos, I. Liontos, E. Skantzakis, B. Förg, D. Charalambidis, and P. Tzallas, APL Photonics **4**, 080901 (2019).
3. M. F. Ciappina, J. A. Pérez-Hernández, A. S. Landsman, W. A. Okell, S. Zherebtsov, B. Förg, J. Schötz, L. Seiffert, T. Fennel, T. Shaaran, T. Zimmermann, A. Chacón, R. Guichard, A. Zaïr, J. W. G. Tisch, J. P. Marangos, T. Witting, A. Braun, S. A. Maier, L. Roso, M. Krüger, P. Hommelhoff, M. F. Kling, F. Krausz, and M. Lewenstein, Rep. Prog. Phys. **80**, 054401 (2017).
4. S. Mikaelsson, J. Vogelsang, C. Guo, I. Sytcevich, A.-L. Viotti, F. Langer, Y.-C. Cheng, S. Nandi, W. Jin, A. Olofsson, R. Weissenbilder, J. Mauritsson, A. L'Huillier, M. Gisselbrecht, and C. L. Arnold, Nanophotonics **10**, 117 (2020).
5. S. Y. Kruchinin, F. Krausz, and V. S. Yakovlev, Rev. Mod. Phys. **90**, 021002 (2018).
6. I. Jiménez-Galán, R. E. F. Silva, O. Smirnova, and M. Ivanov, Optica **8**, 277 (2021).
7. J. Zuo and X. Lin, Laser Photonics Rev. **16**, 2100741 (2022).
8. F. J. Furch, T. Witting, M. Osolodkov, F. Schell, C. P. Schulz, and M. J. J Vrakking, JPhys Photonics **4**, 032001 (2022).
9. T. Nagy, P. Simon, and L. Veisz, Adv. Phys.: X **6**, 1845795 (2021).
10. J. Schulte, T. Sartorius, J. Weitenberg, A. Vernaleken, and P. Russbueldt, Opt. Lett. **41**, 4511 (2016).
11. A.-L. Viotti, M. Seidel, E. Escoto, S. Rajhans, W. P. Leemans, I. Hartl, and C. M. Heyl, Optica **9**, 197 (2022).
12. M. Hanna, F. Guichard, N. Daher, Q. Bournet, X. Délen, and P. Georges, Laser Photonics Rev. **15**, 2100220 (2021).
13. P. Balla, A. Bin Wahid, I. Sytcevich, C. Guo, A.-L. Viotti, L. Silletti, A. Cartella, S. Alisauskas, H. Tavakol, U. Grosse-Wortmann, A. Schönberg, M. Seidel, A. Trabattoni, B. Manschwetus, T. Lang, F. Calegari, A. Couairon, A. L'Huillier, C. L. Arnold, I. Hartl, and C. M. Heyl, Opt. Lett. **45**, 2572 (2020).
14. M. Müller, J. Buldt, H. Stark, C. Grebing, and J. Limpert, Opt. Lett. **46**, 2678 (2021).
15. P. Rueda, F. Videla, T. Witting, G. A. Torchia, and F. J. Furch, Opt. Express **29**, 27004 (2021).
16. L. Daniault, Z. Cheng, J. Kaur, J.-F. Hergott, F. Réau, O. Tcherbakoff, N. Daher, X. Délen, M. Hanna, and R. Lopez-Martens, Opt. Lett. **46**, 5264 (2021).
17. S. Hädrich, E. Shestaev, M. Tschernajew, F. Stutzki, N. Walther, F. Just, M. Kienel, I. Seres, P. Jójárt, Z. Bengery, B. Gilicze, Z. Várallyay, A. Börzsönyi, M. Müller, C. Grebing, A. Klenke, D. Hoff, G. G. Paulus, T. Eidam, and J. Limpert, Opt. Lett. **47**, 1537 (2022).
18. C.-H. Lu, Y.-J. Tsou, H.-Y. Chen, B.-H. Chen, Y.-C. Cheng, S.-D. Yang, M.-C. Chen, C.-C. Hsu, and A. H. Kung, Optica **1**, 400 (2014).
19. P. He, Y. Liu, K. Zhao, H. Teng, X. He, P. Huang, H. Huang, S. Zhong, Y. Jiang, S. Fang, X. Hou, and Z. Wei, Opt. Lett. **42**, 474 (2017).
20. C.-H. Lu, W.-H. Wu, S.-H. Kuo, J.-Y. Guo, M.-C. Chen, S.-D. Yang, and A. H. Kung, Opt. Express **27**, 15638 (2019).
21. M. Seo, K. Tsendsuren, S. Mitra, M. Kling, and D. Kim, Opt. Lett. **45**, 367 (2020).
22. M. Seidel, P. Balla, C. Li, G. Arisholm, L. Winkelmann, I. Hartl, and C. M. Heyl, Ultrafast Science **2022**, 9754919 (2022).
23. M. Seidel, F. Pressacco, O. Akcaalan, T. Binhammer, J. Darvill, N. Ekanayake, M. Frede, U. Grosse-Wortmann, M. Heber, C. M. Heyl, D. Kutnyakhov, C. Li, C. Mohr, J. Müller, O. Puncken, H. Redlin, N. Schirmel, S. Schulz, A. Swiderski, H. Tavakol, H. Tünnermann, C. Vidoli, L. Wenthaus, N. Wind, L. Winkelmann, B. Manschwetus, and I. Hartl, Laser Photonics Rev. **16**, 2100268 (2022).
24. M. Hanna, L. Daniault, F. Guichard, N. Daher, X. Délen, R. Lopez-Martens, and P. Georges, OSA Continuum **4**, 732 (2021).
25. M. Seidel, X. Xiao, S. A. Hussain, G. Arisholm, A. Hartung, K. T. Zawilski, P. G. Schunemann, F. Habel, M. Trubetskov, V. Pervak, O. Pronin, and F. Krausz, Sci. Adv. **4**, eaaq1526 (2018).
26. K. Fritsch, M. Poetzlberger, V. Pervak, J. Brons, and O. Pronin, Opt. Lett. **43**, 4643 (2018).
27. G. Barbiero, H. Wang, M. Graßl, S. Gröbmeyer, D. Kimbaras, M. Neuhaus, V. Pervak, T. Nubbemeyer, H. Fattahi, and M. F. Kling, Opt. Lett. **46**, 5304 (2021).
28. A.-K. Raab, M. Seidel, C. Guo, I. Sytcevich, G. Arisholm, A. L'Huillier, C. L. Arnold, and A.-L. Viotti, Opt. Lett. **47**, 5084 (2022).
29. O. Pronin, M. Seidel, F. Lücking, J. Brons, E. Fedulova, M. Trubetskov, V. Pervak, A. Apolonski, T. Udem, and F. Krausz, Nat. Commun. **6**, 6988 (2015).
30. G. Arisholm and H. Fonnum, "Simulation System For Optical Science (SISYFOS) – Tutorial, Version 2," 21/01183 (Norwegian Defence Research Establishment - FFI, 2021).